KANSAS GEOLOGICAL SURVEY
OPEN-FILE REPORT 2000-71

A Ground-penetrating Radar (GPR) Investigation of the
Oread Limestone, Douglas County, Kansas

by

K. David Newell
Alex Martinez

Disclaimer

The Kansas Geological Survey does not guarantee this document to be free from errors or inaccuracies and disclaims any responsibility or liability for interpretations based on data used in the production of this document or decisions based thereon. This report is intended to make results of research available at the earliest possible date, but is not intended to constitute final or formal publications.

Kansas Geological Survey
1930 Constant Avenue
University of Kansas
Lawrence, KS 66047-3726

A Ground-Penetrating Radar (GPR) Investigation of the Oread Limestone, Douglas County, Kansas

K. David Newell and Alex Martinez
Kansas Geological Survey Open-File Report 2000-71

Summary

Ground-penetrating radar (GPR) was used to image a channel-like feature in the Toronto Limestone (Upper Pennsylvanian, Shawnee Group, Oread Formation) in northeastern Kansas. Although channel-like in appearance, this feature is actually an isolated lens of dolomite in an otherwise light-gray, limestone-dominated stratal unit. The analysis by GPR is an attempt to see the three-dimensional geometry of this diagenetic feature and to determine if this geometry can provide information on the origin of the dolomite

Dipolar, bistatic GPR antennas of 225 MHz and 450 MHz central frequencies were used to collect a 10 m x 5 m 2.5 dimensional common-offset grid, five 10-m-long common-offset profiles, and a common-depth point (CMP) gather. Calculated and measured relative permittivity values of the outcrop rock (10.8-11.1 and 6.7-8.3, respectively), and relatively high GPR signal attenuation, indicated that the limestone contains a significant amount of disseminated siliciclastic material, in addition to a shale at a boundary between major limestone units.

Interpreted GPR common-offset data show an upper wedge-shaped unit thickening northward. The wedge shape is not a depositional feature, but the result of erosion of the top of the unit. This unit has internal stratification resembling cross-bedding, also dipping northward. The dolomitized zone is a north-south trending channel-like feature. It is observable on all GPR lines collected parallel to the outcrop face. The thickening of the dolomitized interval may be due to differential compaction or solution of the dolomite relative to the surrounding limestone beds. Thin-section analysis of selected rock samples indicate the dolomite within the channel-like feature is dominantly a baroque dolomite, which is characteristic of precipitation temperatures in excess of 60° C. The depositional history of the region and local geothermal gradient are not compatible with high-temperature diagenesis in this locality, thus dolomitizing fluids may have conceivably entered the formation by upward movement along fractures. However, no vertical fractures that could facilitate this upward movement of fluid were evident on the outcrop, nor were any fractures detected by GPR.

Introduction

Ground-penetrating radar (GPR) is a near-surface, very-high resolution (centimeters to meters), non-intrusive geophysical technique that employs electromagnetic (EM) energy to image the subsurface (Davis and Annan, 1989). EM energy waves reflect when they encounter a change in dielectric permittivity or

magnetic permeability, and are attenuated by conductivity, which causes the waves to dissipate and transform to heat energy (Davis and Annan, 1989; Olhoeft, 1998). GPR antennas send EM energy pulses into the ground and record reflected energy.

Because it is a relatively rapid and inexpensive technique, GPR is increasingly being used for geologic investigations to extend information into the subsurface from that seen on outcrop or core. Recent outcrop studies of carbonate outcrops include Pratt and Miall (1993), Liner and Liner (1995), Martinez et al. (1998), and McMechan et al. (1998). The central frequencies and bandwidths of the antennas used for a study are importance because they control maximum imaging resolution and penetration depth. Higher frequency antennas provide more detailed images, but less penetration depth. The studies by Pratt and Miall (1993) and Liner and Liner (1995) used relatively low-frequency antennas (50 MHz) to maximize penetration depth. The McMechan et al. (1998) study used several antenna frequencies (50 MHz to 200 MHz) to study karsted dolomites. The Martinez et al. (1998) study used a higher frequency antenna (500 MHz) to investigate two limestone outcrops in northeastern Kansas.

The purpose of this geophysical investigation was to determine if a channel-like feature observed on outcrop in the Upper Pennsylvanian (Virgilian) Toronto Limestone (Shawnee Group, Oread Limestone) (Figure 1) could be imaged using GPR, and if so, what three-dimensional shape did it have. The study site, located in northeastern Kansas (Figure 2), was deemed amenable to GPR because it had minimal soil cover and was easily accessible. A 10 m x 5 m 2.5 dimensional (D) patch of 225 MHz common-offset GPR data, five 10-m-long 450 MHz common-offset GPR data profiles, and a 225 MHz common-mid point (CMP) GPR data gather were collected for this investigation. The 2.5D common-offset patch and five common-offset profiles were centered on the outcrop exposure of the channel-like feature, and covered its full visible extent. A 225 MHz antenna was used for data collection of the 2.5D common-offset patch because it provided optimal penetration depth (maximum of approximately 3 m), imaging resolution (approximately 6 cm), and data collection time for the scales of features to be imaged. The 450 MHz antenna provided greater vertical resolution (approximately 3 cm), but with less penetration depth (maximum of approximately 1.5 m) and greater data collection time. Lower-frequency antennas (i.e., 50 MHz and 100 MHz) were not used because they would not provide sufficient vertical or spatial resolution to image the features of interest in the outcrop rock.

Geologic Background

The Toronto Limestone is an Upper Pennsylvanian (Virgilian) cyclothemic carbonate unit, 2-4 m thick, at the base of the Oread Formation. It represents an intermediate cycle of transgression and regression (Heckel, 1984), on an open-marine carbonate shelf.

The target of this study is peculiar lens-like feature in the Toronto that is exposed on the east side of a road cut on Douglas County Road 13, 1/4 mile south of the Clinton Lake dam (NW NW SE, sec. 20-T.13S.-R.19E.). Prior work by Scott (1990) established that this feature is an isolated lens of brown dolomite in an otherwise light-gray, limestone-dominated stratal unit. This dolomite body is approximately

6 m in width and 2 m thick at maximum. It tapers in thickness laterally and has a slightly convex top and a convex-downward base, thereby having geometry reminiscent of a channel. The top of the dolomite body is bound by a thin (5 cm thick) shale (Scott, 1990). However, unlike a channel, the beds composing the lens appear to grade into adjacent limestone strata, rather than being contained only to the area of the lens. Clark (1990) stated that the dolomite body was not present on the west side of the road cut. Although no lens-like feature is evident on the west side of the road, our field investigations indicate that the Toronto is partly dolomitized over a lateral distance of approximately 10 meters on outcrop across the road from the lens. A northwest-southeast orientation is established if the two dolomitized areas on both sides of the road are lined up.

Outcrop Description

A photomosaic (Plate 1) of the outcrop shows the appearance of the dolomite lens on outcrop. The approximate location of the GPR stations, and location of the samples taken for thin-section analysis also are annotated on this photomosaic. In addition to being expressed as a local thickening of bedding on the outcrop, the dolomitic lens also weathers a darker brown than adjacent limestone strata. The GPR work was done on a ledge above this outcrop. A green plastic container can be seen on this ledge on the photomosaic. An elevation map of the ledge is shown in Figure 3. This map was surveyed with a rod and level and tape measure for the purpose of locating GPR lines.

Rock Samples

Rock samples were taken from the outcrop face from the locations shown in the outcrop photomosaic in Plate 1. These samples were taken to provide petrophysical (via thin-section analysis), and dielectric permittivity (via dielectric probe measurements) information about the outcrop. The thin section billet was then polished again and areas within it were designated their dielectric permittivity. The areas examined for this type of analysis are each approximately 0.5 cm^2.

Thin Section Analyses

Sample 1. Coarse-grained, clay-rich, crinoid-brachiopod packstone, with less than 1% porosity. Porosity is dominantly intraparticle (WP) and microvugular (VUG). Fossil fragments are abraded (average particle size is 1 mm) and well worn, and display overly close packing (embayed and sutured margins where in contact with each other). Most fragments have micrite rims.

Areas microsampled for GPR characteristics are:

A -- mostly crinoid fragments, with local 10% porosity

B -- typical lithology (as in the general description above), but with slightly finer-grained fragments (0.5 to 0.75 mm)

C -- typical lithology (as in the general description above)

Sample 2. Medium-to-coarse grained, clay-rich, phylloid algal-crinoid fragment wackestone, with no porosity. Subsidiary amounts of ostracode, brachiopod, and fusulinid fragments bryozoan fragments; rare sponge spicules and mollusk fragments. Most shell material is delicate and unworn. Ostracodes are not disarticulated. Average particle size is 0.5 mm.

Areas microsampled for GPR characteristics are:

A -- mud-filled burrow devoid of fossils, mostly clay-rich micrite

B, C -- typical lithology (as in the general description above)

Sample 3. Coarse-grained phylloid-algal-brachiopod wackestone. Subsidiary amounts of crinoids and byrozoans are present. Minor amounts of ostracodes and fusulinids are present. Texture and composition is much like #2 above but having very little clay in the matrix. Fossil fragments are unworn and delicate. Matrix muds have clotted appearance and are probably pelleted. There is a trace of WP porosity

Areas microsampled for GPR characteristics are:

A, B, -- typical lithologies (as in the general description above)

C -- a more pelletal area, possibly a burrow, with a gastropod fragment filled with coarse spar, fine grained spar infills the BP porosity between the pellets

Sample 4. Medium-to-coarse grained, clay-rich, phylloid algal-crinoid fragment wackestone. Additional fossil materials present in sample #2 (i.e., ostracodes, brachiopod fragments, fusulinids are not discernable). Average particle size is 0.5 mm. The sample is completely dolomitized with a fine-crystalline dolomite replacing the micrite matrix muds. Clays are present in thin veneers between dolomite crystals. Available WP and VUG porosity (<5% of sample) is filled with medium crystalline baroque dolomite. The sample is thus nonporous.

Areas microsampled for GPR characteristics are all typical of the lithology above, except for C, which has a higher percentage of baroque dolomite and is slightly coarser grained than rest of sample.

Sample 5. Lime mudstone, with sparse crinoid fragments. Minor WP and VUG porosity is filled with medium-crystalline baroque dolomite. The sample is 95% fine-grained dolomite, which replaces the micrite matrix. 1-2% of sample is baroque dolomite, and 2-3% is a late calcite spar. No areas were sampled for GPR characteristics.

Thin Section Interpretations

Samples #3, #2, #1 are from strata outside of the dolomite lens, but they are stratigraphic equivalents of the rocks that constitute the lens (see Figure 3). Sample #3, stratigraphically the lowest of the three samples, represents a quiet open-marine environment, possibly deeper water, without input of fine-grained

siliciclastics (i.e., clays). Sample # 2 represents also represents a quiet open-marine environment, possibly also deep water. Sample #1 represents a high-energy, open marine, with periods of quiet water, possibly a storm deposit. From base to top, these three samples represent a shallowing-upward, open-marine sequence.

The next two samples (#4 and #5) are from the channel-like feature, with #4 being taken at the approximate stratigraphic level as #2. The depositional environments of both samples #2 and #4 are interpreted to be similar -- a quiet open-marine environment, possibly deeper water. Thin section #5 is also interpreted to be a low energy, open-marine environment.

Baroque dolomite is interpreted to form in a moderately high temperature environment of at least 60 °C, and possibly as high as 150 °C (Radke and Mathis, 1980). It is considered a subset of a class of burial dolomite called "late dolomite cement", or "LDC". LDC is associated with Mississippi Valley-type (MVT) mineralization present throughout southeastern Missouri and west into Kansas and Oklahoma in Paleozoic strata (Leach et al., 1991). Northward advective migration of hot brines out of the Arkoma and Anadarko basins in late Pennsylvanian -- Early Permian time may be the cause of much of the MVT mineralization in the southern Mid-continent (Leach and Rowan, 1986; Gregg and Shelton, 1990).

The depth of burial of this locality is cannot be precisely determined, but a regional study of the thermal and tectonic history of the Cherokee basin in Förster et al. (1998) suggests that temperature the base of the Shawnee Group may have experienced during its maximum burial in Early Permian time was only approximately 45 °C. It is thus difficult to explain why such baroque dolomite is so pervasive in the Toronto Limestone at this locality. One possibility is that it could be the result of dolomitizing fluids that may have come up through fractures. Although the lens-like feature is localized, no vertical fractures are evident on outcrop (Figure 3).

Dielectric Measurement Results

Measurements taken using a dielectric probe record both the real (relative permittivity or dielectric constant; ε_r), and imaginary (dielectric loss; ε_i) portions of the dielectric permittivity. The real portion of dielectric permittivity is what can be calculated from GPR CMP velocity information (see below). Dielectric constant measurements made with a dielectric probe are useful as a check for dielectric constant values calculated from CMP gathers. The imaginary portion of dielectric permittivity is related to conductivity, and hence attenuation of GPR signal energy.

Measurement Procedure

A HP 85070A dielectric probe was used to measure dielectric constants from the rock samples. Prior to measurements, the rock samples were cut and polished to provide a smooth face for the dielectric probe tip and reduce experimental error. Dielectric constant measurement was performed using the procedure described in Martinez and Byrnes (1999). At least three measurements were taken from each sample to determine small-scale variability within the rock. Measurements were at fixed frequency intervals, ranging

from 25 MHz to 1.5 GHz, in 25 MHz steps. The measured dielectric data were stored in ASCII format and exported to a spreadsheet for analysis. The based on repeat measurements at the same sample locations, accuracy of dielectric constant measurements was within 0.05.

Measurement Results

The results of the dielectric measurements are summarized below in Table 1 and in Figure 4.

Table 1. Results of dielectric constant measurements and thin section analysis.

Sample	ε_r range	ε_r average	Porosity	Lithology
1	6.7-7.0	6.8	<1%; Porosity is dominantly intraparticle (WP) and micruvugular (VUG).	Coarse-grained, clay-rich, crinoid-brachiopod packstone. Fossil fragments are abraded (average particle size is 1 mm) and well worn, and display overly close packing (embayed and sutured margins where in contact with each other). Most fragments have micrite rims.
2	4.6-8.3	7.3	0%	Medium-to-coarse grained, clay-rich, phylloid algal-crinoid fragment wackestone. Subsidiary amounts of ostracode, brachiopod, and fusulinid fragments bryozoan fragments, rare sponge spicules and mollusk fragments. Most shell material is delicate and unworn. Ostracodes are not disarticulated. Average particle size is 0.5 mm.
3	7.9-8.0	7.9	~0%; There is a trace of WP porosity	Coarse-grained phylloid-algal-brachiopod wackestone. Subsidiary amounts of crinoids and byrozoans are present. Minor amounts of ostracodes and fusulinids are present. Texture and composition is much like #2 above but having very little clay in the matrix. Fossil fragments are unworn and delicate. Matrix muds have clotted appearance and are probably pelleted.
4	7.1-7.4	7.2	0%; Available WP and VUG porosity (<5% of sample) is filled with medium crystalline baroque dolomite. The sample is thus nonporous.	Medium-to-coarse grained, clay-rich, phylloid algal-crinoid fragment wackestone. Additional fossil materials present in sample #2 (i.e., ostracodes, brachiopod fragments, fusulinids are not discernable). Average particle size is 0.5 mm.

				The sample is completely dolomitized with a fine-crystalline dolomite replacing the micrite matrix muds. Clays are present in thin veneers between dolomite crystals.
5	---	---	0%; Minor intraparticle (WP) and microvugular (VUG) porosity is filled with medium-crystalline baroque dolomite.	Lime mudstone, with sparse crinoid fragments. The sample is 95% fine-grained dolomite, which replaces the micrite matrix. 1-2% of sample baroque dolomite, and 2-3% being a late calcite spar.

GPR Data

Site Preparation and Survey Design

The study site consisted of a 10 m (in-line) x 5 m (cross-line) area beginning approximately 0.5 m behind the outcrop face, with an in-line orientation of north 42° west (Figure 3, Plate 1). The 10 m in-line extent was chosen because it encompassed the entire outcrop exposure of the channel-like feature.

Site preparation consisted of clearing debris (mainly vegetation and small rocks) from the top of the outcrop, and flagging the ends of the antenna pathways. Clearing the pathways of debris aided in collection of relatively straight GPR profiles and helped the antennas to better couple with the ground. A level and rod were used to gather relative elevation information necessary for elevation corrections of the GPR data.

The GPR equipment consisted of a Sensors and Software PulseEkko 1000 unit with 225 MHz and 450 MHz dipolar, bistatic antennas. The 225 MHz antenna was used to collect 10-m-long common-offset profiles every 0.5 m parallel to the outcrop face. This resulted in a 2.5D grid composed of eleven 225 MHz common-offset profiles. The 450 MHz antenna was used to collect 10-m-long common-offset profiles every 1.0 m parallel to the outcrop face. This resulted in six 450 MHz common-offset lines being gathered. The 450 MHz common-offset data were used to provide high-resolution images to aid in the interpretation of the 225 MHz data. Additional 450 MHz data were not collected due to their limited imaging depth (a maximum of approximately 1.5 m). A single 225 MHz CMP gather was collected parallel to line 2.5, centered on station 6.0 in order to provide data for velocity analysis (see below). This site was chosen because it is a relatively flat region near the center of the data set. A summary of acquisition parameters for each data type and antenna is given below in Table 2.

Table 2. Summary of GPR data acquisition parameters

Data type	Antenna center frequency (MHz)	Sample interval (ns)	Record length (ns)	Antenna offset (m)	Trace spacing (m)	Line spacing (m)
Common-offset	225	0.2	200	0.5	0.10	0.5
	450	0.2	200	0.25	0.05	1.0
Common-mid point	225	0.2	200	0.25–3.25	0.10	n/a

GPR Data Processing

The GPR data were downloaded from the GPR unit and imported into Seismic UNIX (SU, a shareware seismic processing program from the Colorado School of Mines) for digital signal processing. Different processing steps were taken for the 225 MHz common-offset data, 450 MHz common-offset data, and 225 MHz CMP data.

Data processing of the 225 MHz common-offset data consisted of bandpass filtering, normal move-out (NMO) and dip move-out (DMO) corrections, migration, elevation corrections, and trace balancing and gaining. Bandpass filters were designed according to the 225 MHz bandwidth of the antenna (112.5 MHz to 337.5 MHz). They were used to remove DC-bias inherent to GPR data, and low- and high-frequency noise outside of the antenna bandwidth. Because the antennas were at a fixed distance of 0.5 m apart during data collection, NMO corrections were used to correct the data to a zero offset. This had the added advantage of removing the direct-air and direct ground waves from the common-offset record via a stretch mute. The NMO velocity function used was 0.090 m/ns, which was obtained from velocity analysis of the 225 MHz CMP gather (see below). The same velocity function was used for migration and elevation corrections. Migration of the data aided in making some reflections more continuous and distinct. Elevation corrections resulted in the data mimicking topography and becoming more interpretable. Gaining and trace balancing were performed using two different methods. The first method involved using an automatic gain control (AGC) with a 25 ns window and Gaussian taper in order to enhance reflection information from the later portions of the data record. The second gaining method used the parameters discussed in Claerbout (1985): multiplying the data by time-squared, taking the square root of the scaled data, and clipping amplitude values of the upper 95% of the amplitude range. These gaining and balancing parameters had the advantage of showing areas of decreased signal strength (i.e., increased attenuation) across the common-offset profiles, which is useful for lithologic-induced attenuation analysis. However, these parameters did not sufficiently enhance reflection information from the later portions of the record. A time gate of 100 ns was used to reduce the record length, and thereby file size, because no useful information was recorded later. The two processed 225 MHz common-offset data sets were exported from SU as SEGY 3D data volumes for importation into a seismic interpretation software package.

The processing of the 450 MHz common-offset data differed from the 225 MHz data in that frequency-wavenumber (f-k) filters were used to remove horizontal events prior to bandpass filtering, and the

bandpass filter parameters were designed for the 450 MHz antenna. Truly horizontal events usually are not reflections, but rather the direct ground wave, direct air wave, and instrumentation-related noise. The 450 MHz antenna recorded significant system-related noise, especially when compared to the 225 MHz antenna. This was possibly due to extreme heat (above 100 degrees Fahrenheit) during collection of the 450 MHz data. The system-related noise had constant arrival times, resulting in horizontal events on the common-offset records. The f-k filters were designed to remove events centered on the zero-k axis in f-k space, and effectively the horizontal system-related noise. The bandpass filters for the 450 MHz common-offset data were designed to remove frequencies outside the bandwidth of the antenna (225 MHz to 675 MHz). The same gaining parameters as the 225 MHz common-offset data were used for the 450 MHz common-offset data. Although no useful reflection information was recorded beyond approximately 50 ns on the 450 MHz common-offset data records, a time-gate of 100 ns was used to reduce the length to the same as that of the 225 MHz common-offset data records. This aided in SEGY data loading into the interpretation software. The two 450 MHz common-offset data sets were exported from SU as SEGY 2D lines for importation into a seismic interpretation software package.

The 225 MHz CMP data processing consisted of bandpass filtering, NMO corrections, and gaining. The bandpass filter used for this data set was the same as the one used for the 225 MHz common-offset data set. The NMO corrections allowed velocity analysis to be performed, providing information concerning the velocity of the outcrop rock. The gain applied to the CMP data consisted of an AGC with a 25 ns window and Gaussian taper. This aided in identifying reflection information in the latter part of the record.

GPR Data Interpretation

CMP Gather

The 225 MHz CMP gather was obtained in order to provide velocity data necessary for elevation corrections and common-offset data interpretation (Figure 5(a)). The CMP gather was centered on line 2.5, station 6.0, and had a maximum antenna separation of 3.25 m (Figure 5).

Identifiable on the CMP gather were the direct airwave, the direct ground-coupled wave, a refracted ground-coupled wave, and several reflections (Figure 5(b)). The direct airwave had a velocity of 0.3 m/ns, and the direct and refracted ground-coupled waves had a velocity of 0.098 m/ns. The reflections were NMO corrected, providing a velocity function for the study site (Figure 5(c)). The NMO velocity function (approximately average velocity) is shown in Figure 5 and is between 0.085 and 0.090 m/ns.

Interval velocity values were calculated from the average velocity values obtained from the CMP gather using the Dix equation. These velocity values are lower than 0.11 m/ns, the value commonly reported for limestone (Davis and Annan, 1989; Daniels, 1996). Dielectric constant values for the site can be calculated from velocity using the relationship $\varepsilon_r = [(3\times10^8 \text{ m/s}) / (V_{interval})]^2$. Using this equation results in measured ε_r values of 10.8 to 11.1 (limestone), and 81.7 (shale). Reported ε_r values for limestone range from 4-8 (Davis and Annan, 1989; Daniels, 1996), but do not state how homogeneous the limestone is. Assuming

the reported values are for relatively homogeneous limestone, the calculated ε_r values may indicate that the limestone at the study site contains a significant amount of disseminated clays or siliciclastic material (e.g., shale). Another indication of significant disseminated siliciclastic material in the limestone is the relatively rapid attenuation in signal strength seen on the GPR data. The high value for the shale layer indicates that it is highly reflective (as can be seen on the 450 MHz common-offset data), therefore most wave energy is reflected and only a small portion is transmitted. Additionally, the shale is most likely highly attenuative, therefore absorbing most of the transmitted energy.

Common-Offset Profiles

Diffractions and Out-of-Plane Reflections

The GPR data contain several diffractions caused by the EM waves encountering nearby tree trunks (see GPR Line 4.0 – 225 MHz in Figure 6). Tree trunk diffractions are most prominent on the data the farthest away from the outcrop, and closest to the trees. This cultural noise is easily identifiable because of its linear shape, and constant move-out velocity of 0.3 m/ns (the velocity of EM waves in air).

The outcrop interface appears to be causing out-of-plane reflections on line 0.0 (which is 0.5 m behind the outcrop face), and possibly on line 0.5 (which is 1.0 m behind the outcrop face) (see GPR Line 0.0 - 225 MHz in Figure 6). Using the frequency extremes of each antenna (113 MHz and 337 MHz for the 225 MHz antenna; 225 MHz and 675 MHz for the 450 MHz antenna) and a velocity of 0.090 m/ns, it is possible to calculate Fresnel zone radii for each antenna (Figure 7). For the 225 MHz data, a Fresnel zone radius of 0.5 m is reached at a depth of 1.5 m in-line, and 3 m cross-line. As shown in Figure 7, the Fresnel zone radii increase inversely with frequency. This may explain the relatively high noise level of the lower portion of the 225 MHz data from line 0.0 (Figure 6), which have reduced frequency content due to high-frequency signal attenuation. The 450 MHz data have a higher frequency content, and therefore have a smaller Fresnel zone (Figure 7(c)).

Reflections

The interpretation divided the subsurface into three distinct zones: an upper, capping unit; the channel-like feature; and the unit enclosing the channel-like feature.

The upper unit is correlative to a limestone bed capping the channel-like feature (see blue reflection on Plate 1). The base of this unit is imaged as a strong, continuous reflection. Within the upper limestone are northwesterly dipping reflections that are interpreted to be the result of cross-bed-like features. Some of these are observable on outcrop. In the GPR sections (Figure 6), this package resembles a northwesterly dipping wedge. This apparent wedge primarily is due to differential erosion at the top of the outcrop.

The channel-like feature is correlative with dipping reflections that dip into a region with chaotic reflection character. The dipping reflections that flank the chaotic reflections are gentle on the southeast side and steeper on the northwest. The base of the channel-like feature is difficult to image, but can be

defined as the transition from the overlying chaotic reflection character to the underlying more continuous reflection character.

The unit enclosing the channel is characterized by relatively continuous reflections that are oriented parallel to the base of the unit overlying the channel-like feature. These reflections are likely due to thin, shaly intervals between thicker limestone beds.

Frequency Spectra and Attenuation

Frequency and f-k spectra of the data sometimes can be used to further aid investigations of changing lithology. This is because increases in conductivity can result in downward shifts in recorded central frequency of antennas (Daniels, 1996), and increases in DC-bias (Annan, 1996). The frequency spectra of the data from the study site exhibit several interesting trends. The frequency content of the data vary in a systematic manner across the outcrop length, and appear to be related to the amount of shale at the base of the upper limestone. The lateral position of an increase in shale content that is observed on the outcrop can be traced beyond the outcrop via observing frequency spectra.

The gaining method of Claerbout (1985) allowed differences in EM signal attenuation to be observed along the common-offset data profiles. In many instances, differences in attenuation may be attributed to changes in lithology of the material through which the EM wave is traveling. When the GPR frequency spectra exhibit a downward shift, and the data are highly attenuated, the rock contains more shale at the bounding surfaces, and possibly more disseminated shale within it.

Conclusions

The large-scale (8 m wide, 2 m thick) channel-like feature seen on outcrop was capable of being imaged using GPR. From interpretations of the GPR data, the channel-like feature appears to trend north-south. Unfortunately, only a portion of the feature was imaged because the study area did not extend further to the north. A small-scale (2 m wide, 0.25 m thick) channel within the upper limestone was also successfully imaged. This channel found to also trend north-south.

Although this feature at first appearance resembles a channel, it is actually a locally dolomitized area in the Toronto Limestone. Strata largely composed of medium-grained wackestone is laterally replaced by dolomite over a distance of about one meter. The dolomitized area is approximately 50% thicker than the correlative adjacent strata, and this thickening thus gives a channel-like morphology to this geologic feature. Thin sections indicate the dolomite is a replacive, dominantly a baroque dolomite. Baroque dolomite is indicative of relatively high-temperature conditions (i.e., at least 60 °C). The burial history of the area cannot easily account for such a temperature, but perhaps movement of hot fluids locally up through joints and fractures could account for such an isolated dolomitized area on the outcrop. The most likely time for such movement of hot fluid was during the Ouachita orogeny in Pennsylvanian-Permian time.

There were two indicators from the GPR data that the limestone at the study site contains a significant amount of disseminated clastic material. The velocities of the limestone are very slow when compared to reported values for limestone, meaning it is not homogeneous calcium carbonate. Additionally, the rapid attenuation of the GPR signal indicates relatively high conductivity, thus the limestone is not pure limestone but contains a significant amount of other more conductive material. Differences in signal attenuation along the common-offset profiles indicate changes in lithology, especially within the channel-like fill.

If GPR data were collected when the outcrop is fully saturated with water, then the velocity differences between relatively non-porous and porous strata would likely be result in better imaging of this feature. This is because the water in the more porous strata would decrease the overall EM velocity.

Acknowledgments

Colin Robins provided geophysical field assistance for this study. Alan Byrnes aided in measurement of dielectric constants from rock samples. Jason Cansler aided in drafting figures. Seismic Micro-Technologies (SMT) provided the Kingdom Suite interpretation software through an educational grant to the University of Kansas.

References

Annan, A. P., 1996, Ground-penetrating workshop notes: Sensors and Software, Inc., Mississauga, Ontario.

Claerbout, J. F., 1985, **Imaging the Earth's interior**: Blackwell-Science-Incorporated, 233-236.

Daniels, D. J., 1996, Surface-penetrating radar: IEE Radar, Sonar, Navigation and Avionics Series 6, E. D. R. Sharman and P. Bradsell, eds., Short Run Press Ltd., Exeter, United Kingdom.

Davis, J. L. and A. P. Annan, 1989, Ground-Penetrating Radar for High-Resolution Mapping of Soil and Rock Stratigraphy: Geophysical Prospecting **37**, 531-551.

Förster, A., D. F. Merriam, and P. Hoth, 1998, Geohistory and thermal maturation in the Cherokee basin (Mid-Continent, U.S.A.): results from modeling: American Association of Petroleum Geologists **82**, no. 9, 1673-1693.

Gregg, J. M., and K. L. Shelton, 1990, Dolomitization and dolomite neomorphism in the back reef facies of the Bonneterre and Davis Formations (Cambrian), southeastern Missouri: Journal of Sedimentary Petrology **60**, no. 4, 549-562.

Heckel, P. H., 1984, Factors in mid-continent Pennsylvanian limestone deposition: Limestones of the Mid-Continent, N. J. Hyne, ed., Tulsa Geological Society, Special Publication no. 2, 25-50.

Leach, D. L., G. S. Plumlee, A. H. Hofstra, G. P. Landis, E. L. Rowan, and J. G Viets, 1991, Origin of late dolomite cement by CO_2-saturated deep basin brines; evidence from the Ozark region, central United States: Geology **19**, no. 4, 348-351.

Leach, D. L., and E. L. Rowan, 1986, Genetic link between Ouachita foldbelt tectonism and the Mississippi Valley-type lead-zinc deposits of the Ozarks: Geology **14**, no. 11, 931-935.

Liner, C. L., and J. L. Liner, 1995, Ground penetrating radar: a near-face experience from Washington County, Arkansas: The Leading Edge **14**, no. 1, 17-21.

Martinez, A., J. M. Kruger, and E. K. Franseen, 1998, Utility of using ground-penetrating radar for near surface high-resolution imaging of Lansing-Kansas City (Pennsylvanian) limestone reservoir analogs: Current Research in the Earth Sciences, Kansas Geological Survey, Bulletin 241, part 3, 43-59.

Martinez, A., and A. Byrnes, 1999, Measurement procedure for rock samples using the HP7050A dielectric probe: Kansas Geological Survey, Open-file Report 99-01, 17 p.

McMechan, G. A., R. G. Loucks, X. Zeng, and P. Mescher, 1998, Ground penetrating radar imaging of a collapsed paleocave system in the Ellenburger dolomite, central Texas: Journal of Applied Geophysics **39**, 1-10.

Olhoeft, G. R., 1998, Electrical, magnetic and geometric properties that determine ground-penetrating radar performance: Proceedings from the 7th international conference on ground-penetrating radar, 177-182.

Pratt, B. R., and A. D. Miall, 1993, Anatomy of a bioclastic grainstone megashoal (Middle Silurian, southern Ontario) revealed by ground-penetrating radar: Geology **21**, no. 3, 223-226.

Radke, B. M., and R. L. Mathis, 1980, On the formation and occurrence of saddle dolomite: Journal of Sedimentary Petrology **50**, no. 4, 1149-1168.

Scott, S K., 1990, Analysis of a channel-shaped dolomite lens in the Toronto Limestone in Douglas County, Kansas: The Compass 67, no. 3, 175-179.

List of Figures

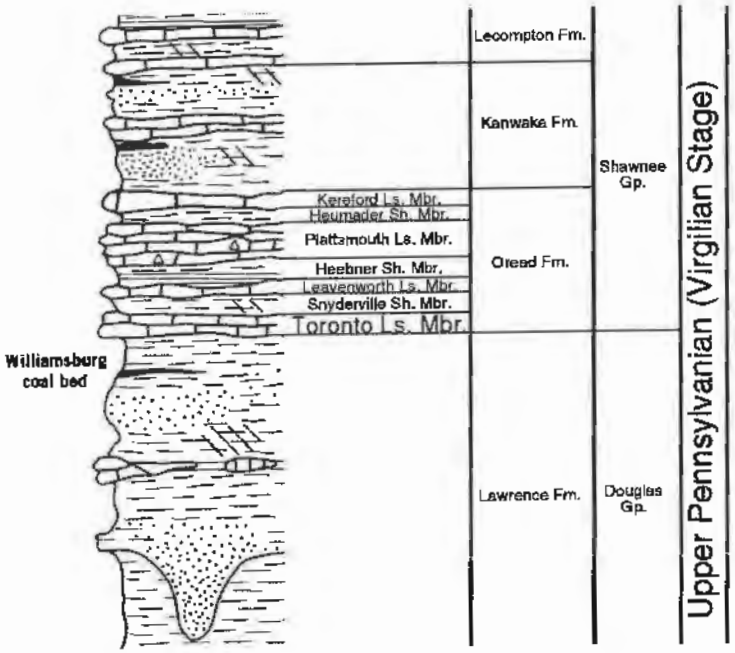

Figure 1. Stratigraphic column. The Toronto Limestone is the focus of this study.

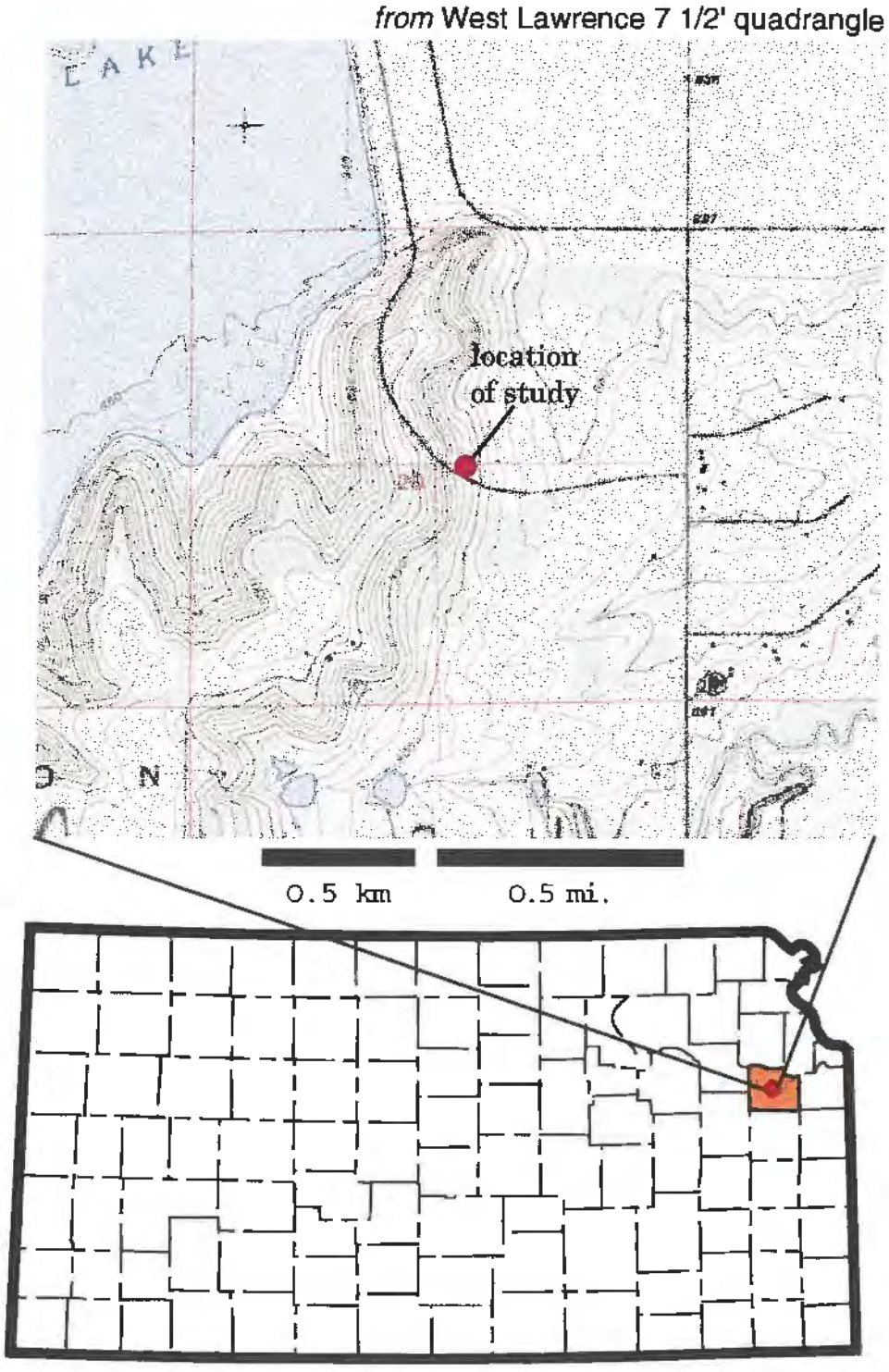

Figure 2. Location of the study -- Douglas County Road 13, 1/2 mile south of Clinton Lake Dam; NW NW SE section 20-T.13S.-R.19E.

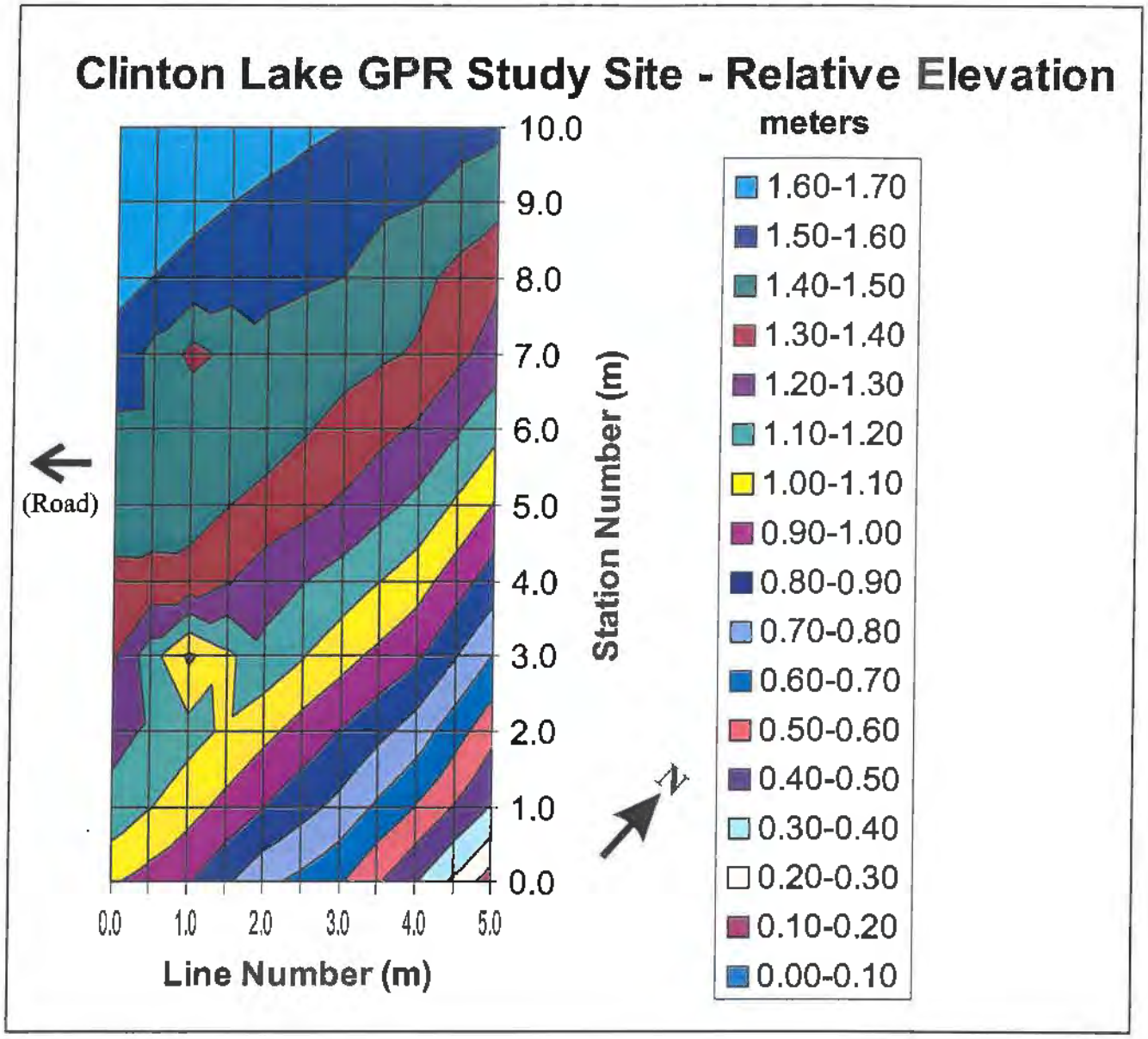

Figure 3. Clinton Lake GPR study site.

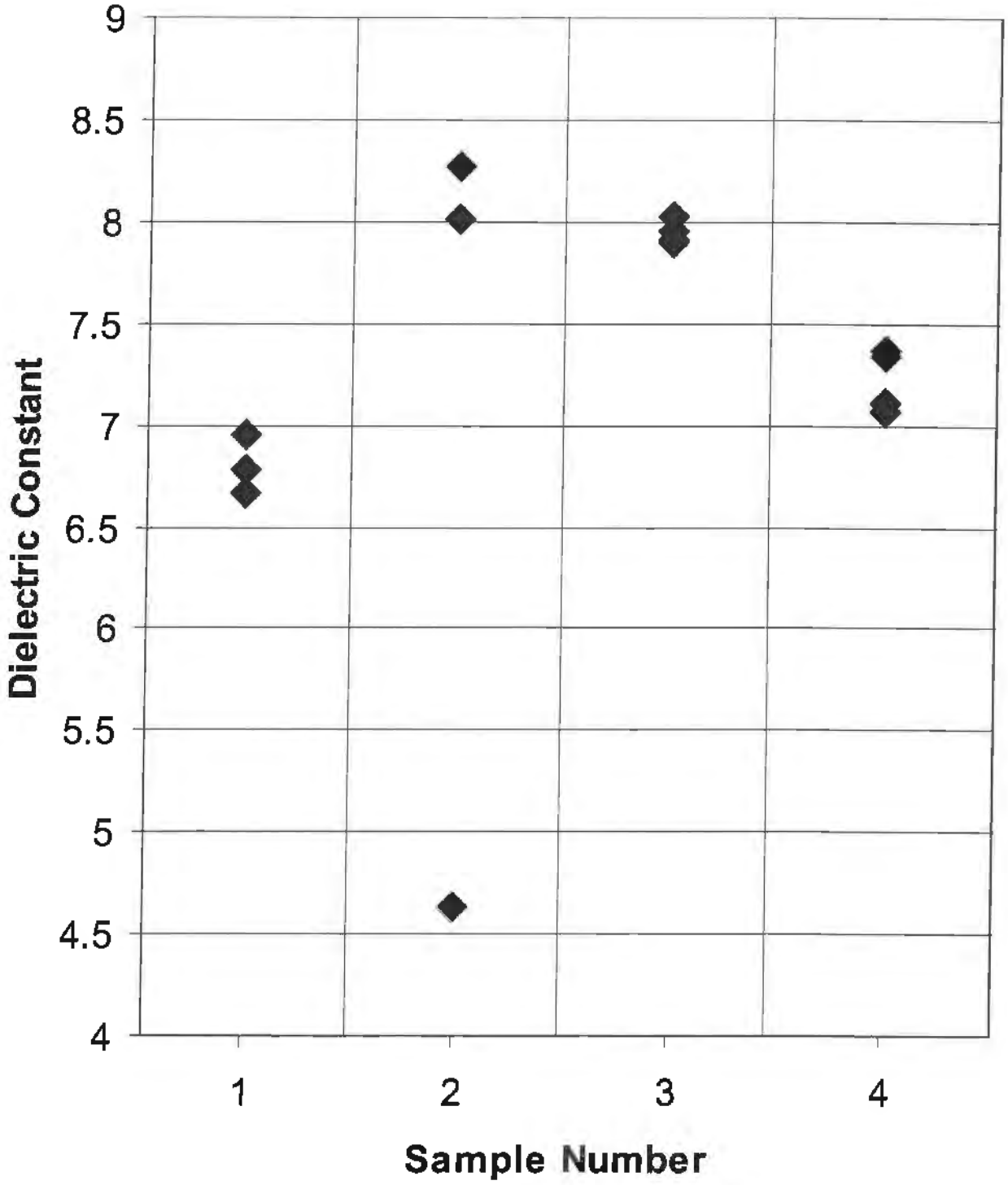

Figure 4. Dielectric constants. Plot of measured dry dielectric constant values (averaged over 750 to 1500 MHz) for each sample from the Clinton Lake study site (see Plate 1 for sample locations). Sample 2 exhibited the most dielectric variability, with one measurement value from a siderite nodule (?) of 4.6.

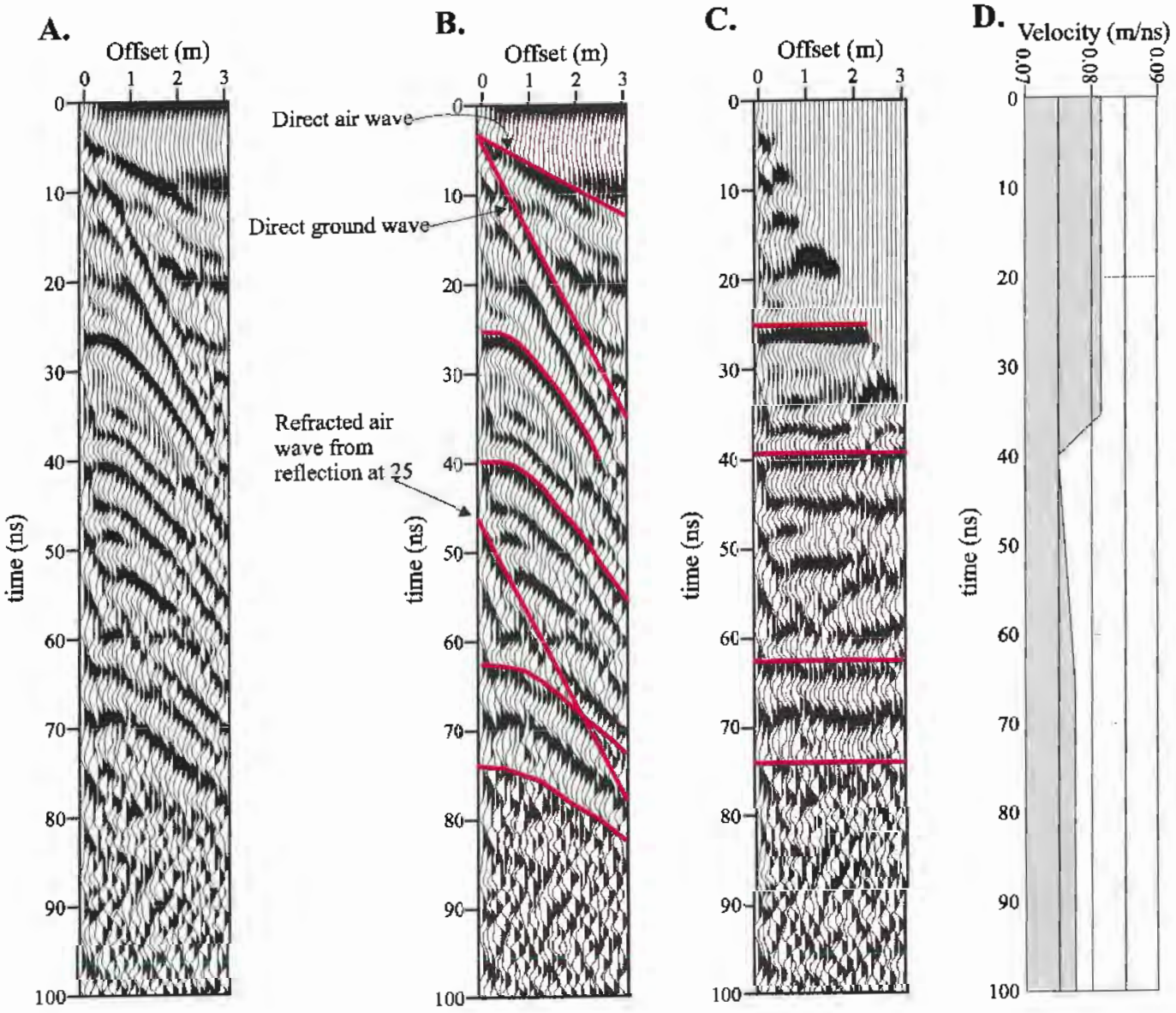

Figure 5. CDP data. (A) Common depth-point (CDP) gather from Line 2.5, Station 6.0, with a trace spacing of 0.1 m. (B) Interpreted CDP gather. The locations of the direct air, direct ground, and refracted air waves are indicated by arrows. Several of the reflections also seen on the common-offset data are shown by lines. (C) Normal move-out (NMO) corrected CDP gather. (D) Velocity function derived from NMO corrections.

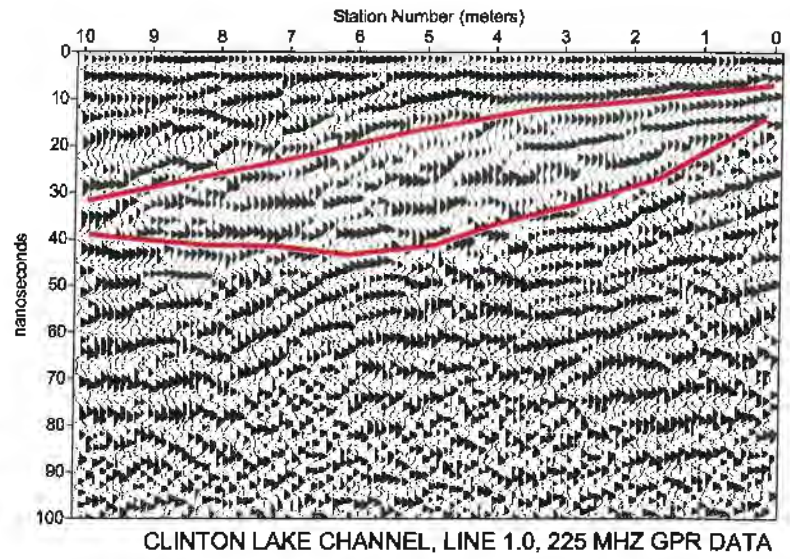

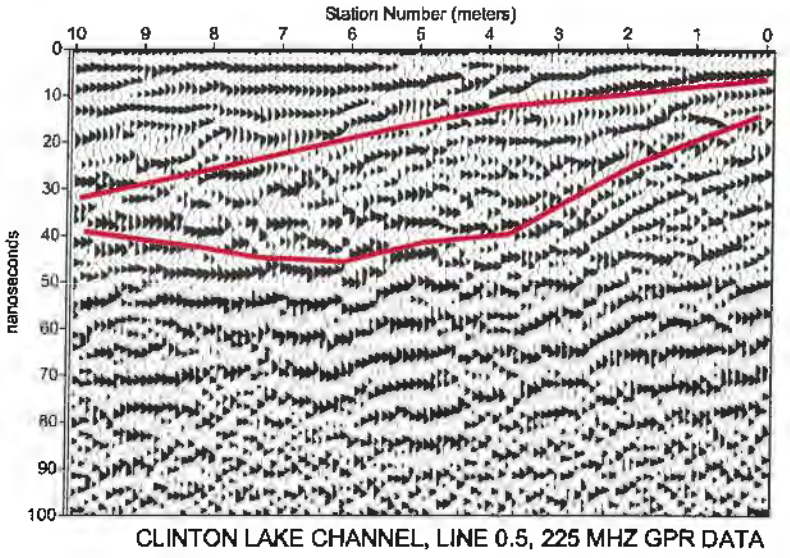

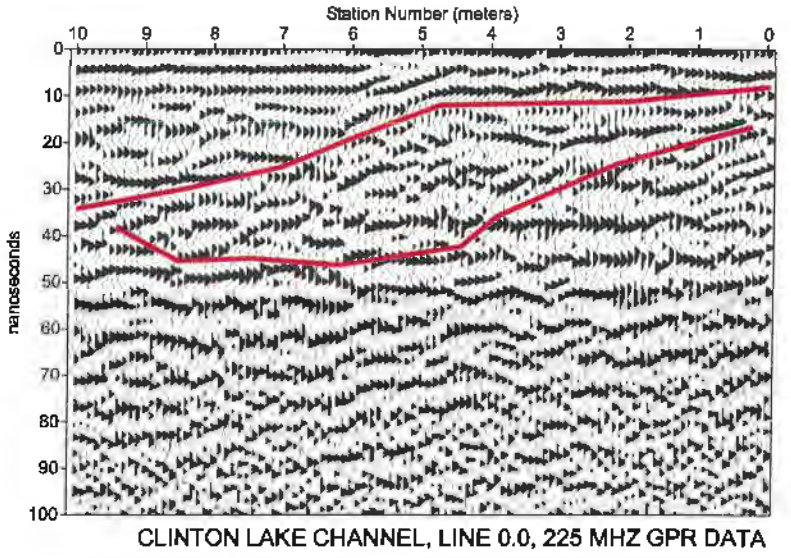

Figure 6. GPR lines 0.0, 0.5 and 1.0.

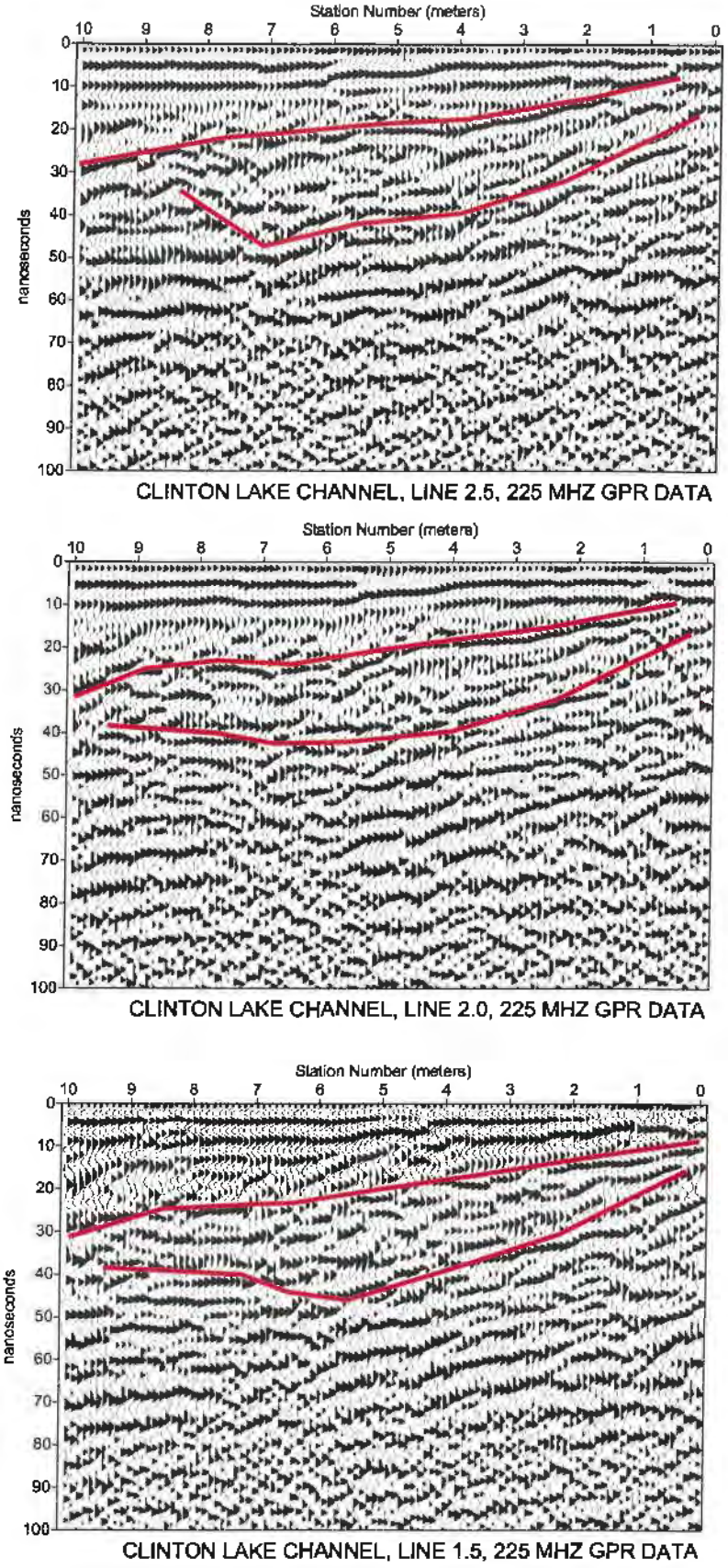

Figure 6 (continued). GPR lines 1.5, 2.0 and 2.5.

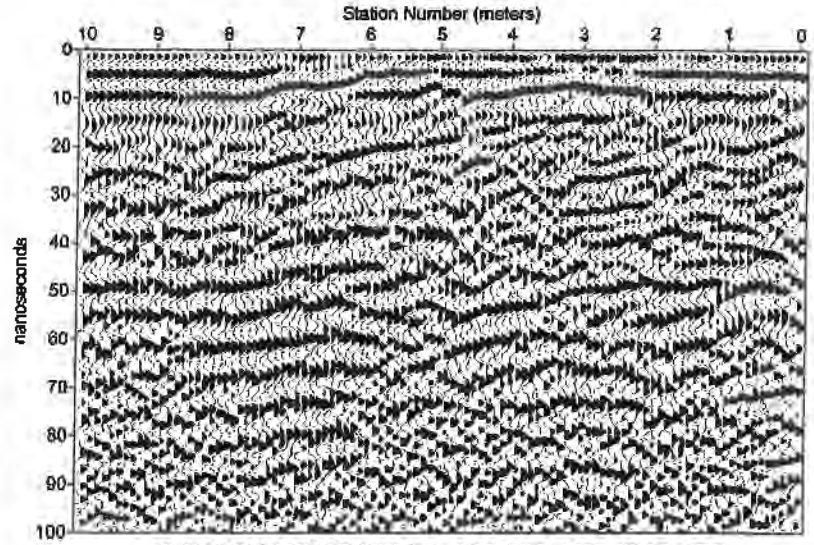

CLINTON LAKE CHANNEL, LINE 4.0, 225 MHZ GPR DATA

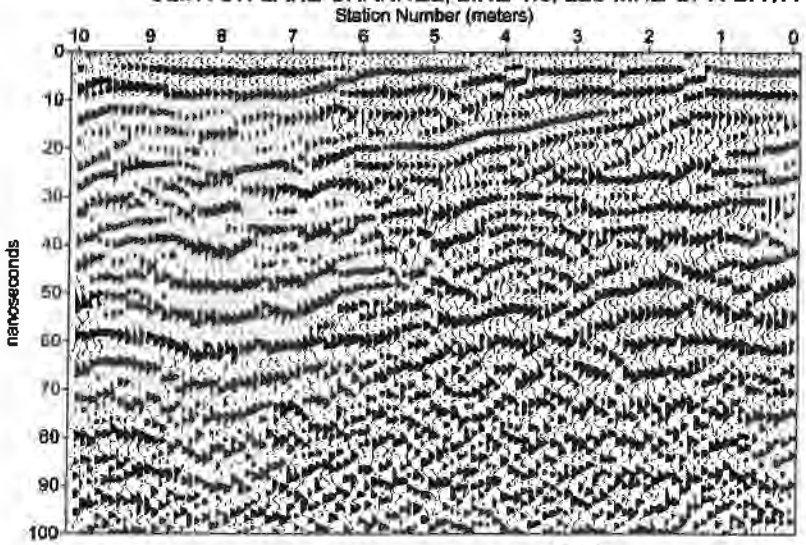

CLINTON LAKE CHANNEL, LINE 3.5, 225 MHZ GPR DATA

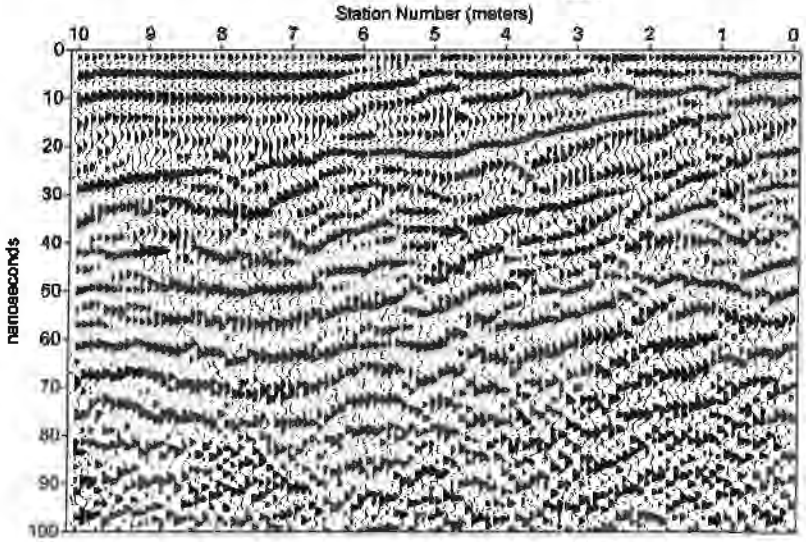

CLINTON LAKE CHANNEL, LINE 3.0, 225 MHZ GPR DATA

Figure 6 (continued). GPR lines 3.0, 3.5 and 4.0.

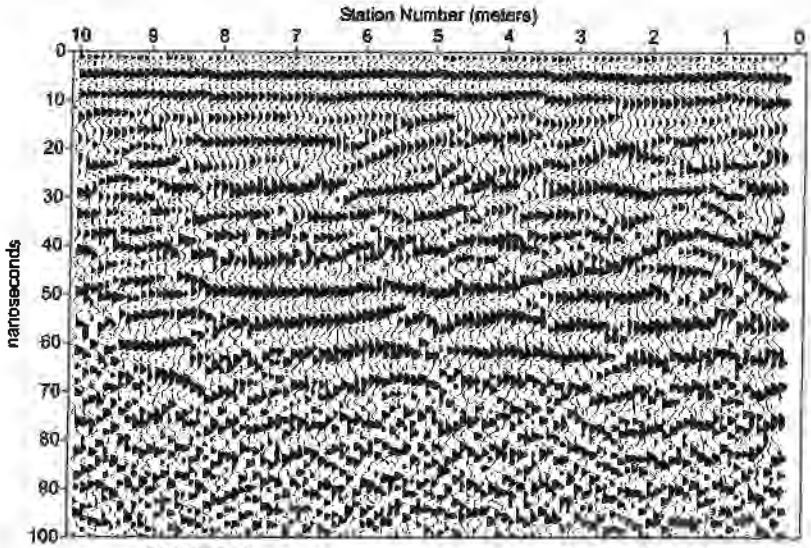

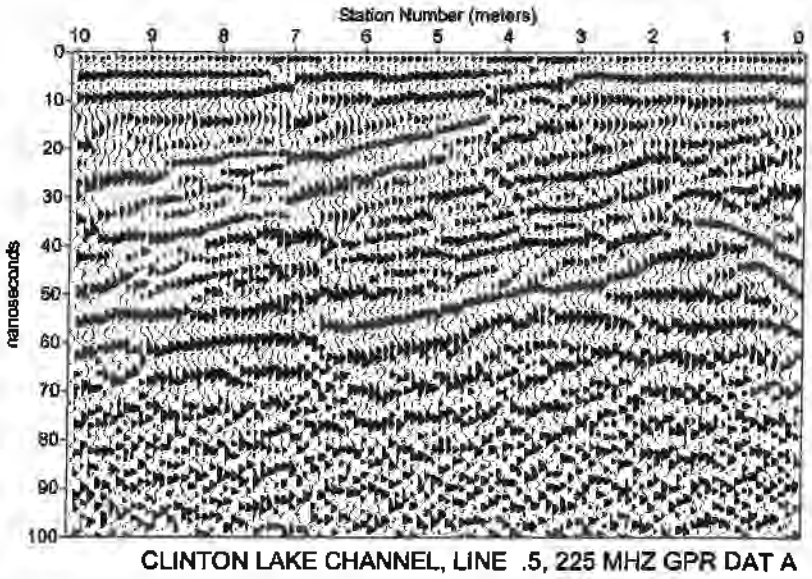

Figure 6 (continued). GPR lines 4.5 and 5.0.

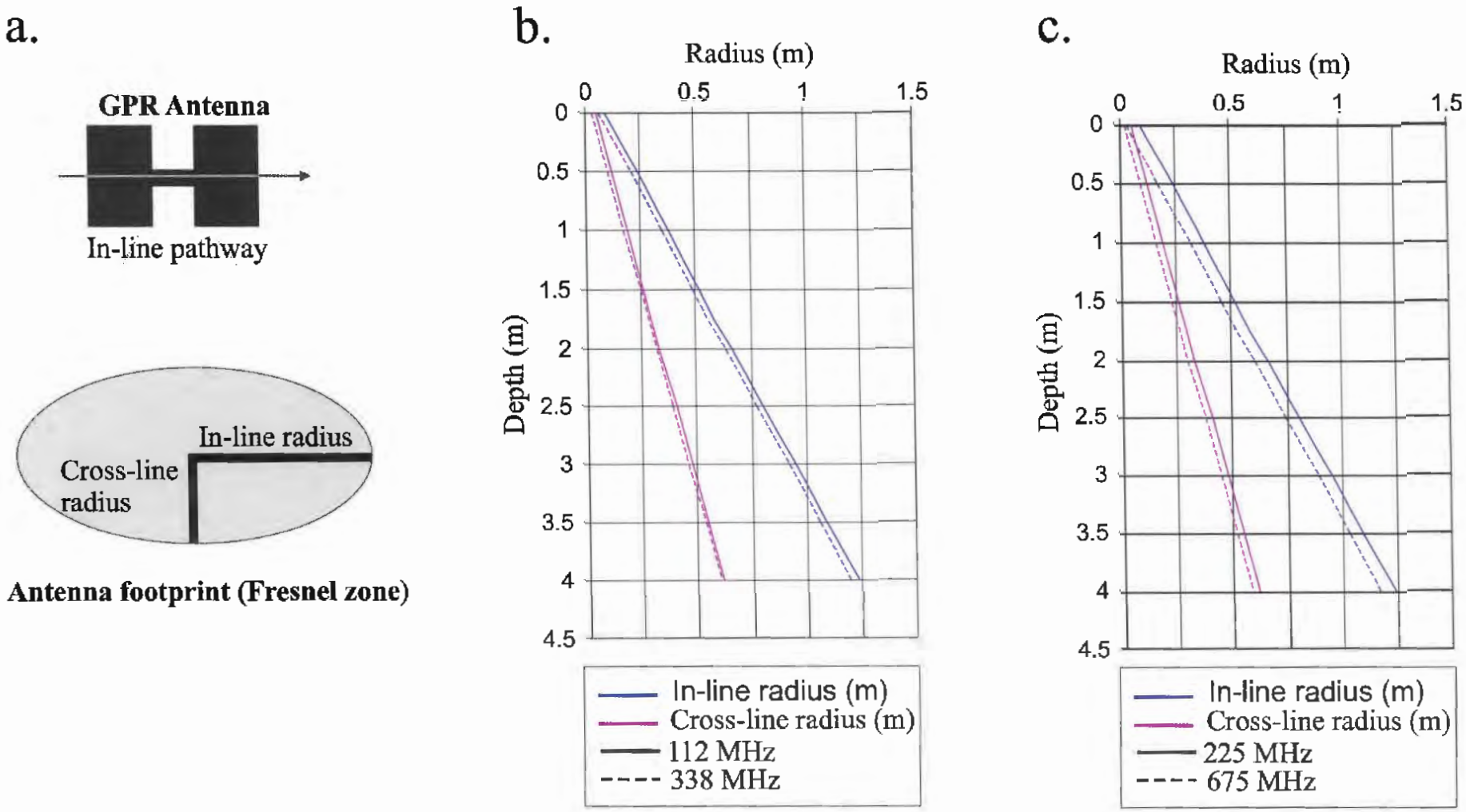

Figure 7. Fresnel Zone. (a) Diagram of a GPR antenna and its antenna footprint (Fresnel zone). The Fresnel zone of a GPR antenna is elliptical in shape, with the in-line radius being twice the cross-line radius (Annan, 1996). (b) Minimum and maximum Fresnel zone radii for the 225 MHz center frequency antenna using a velocity of 0.0825 m/ns. (c) Minimum and maximum Fresnel zone radii for the 450 MHz center frequency antenna using a velocity of 0.0825 m/ns.

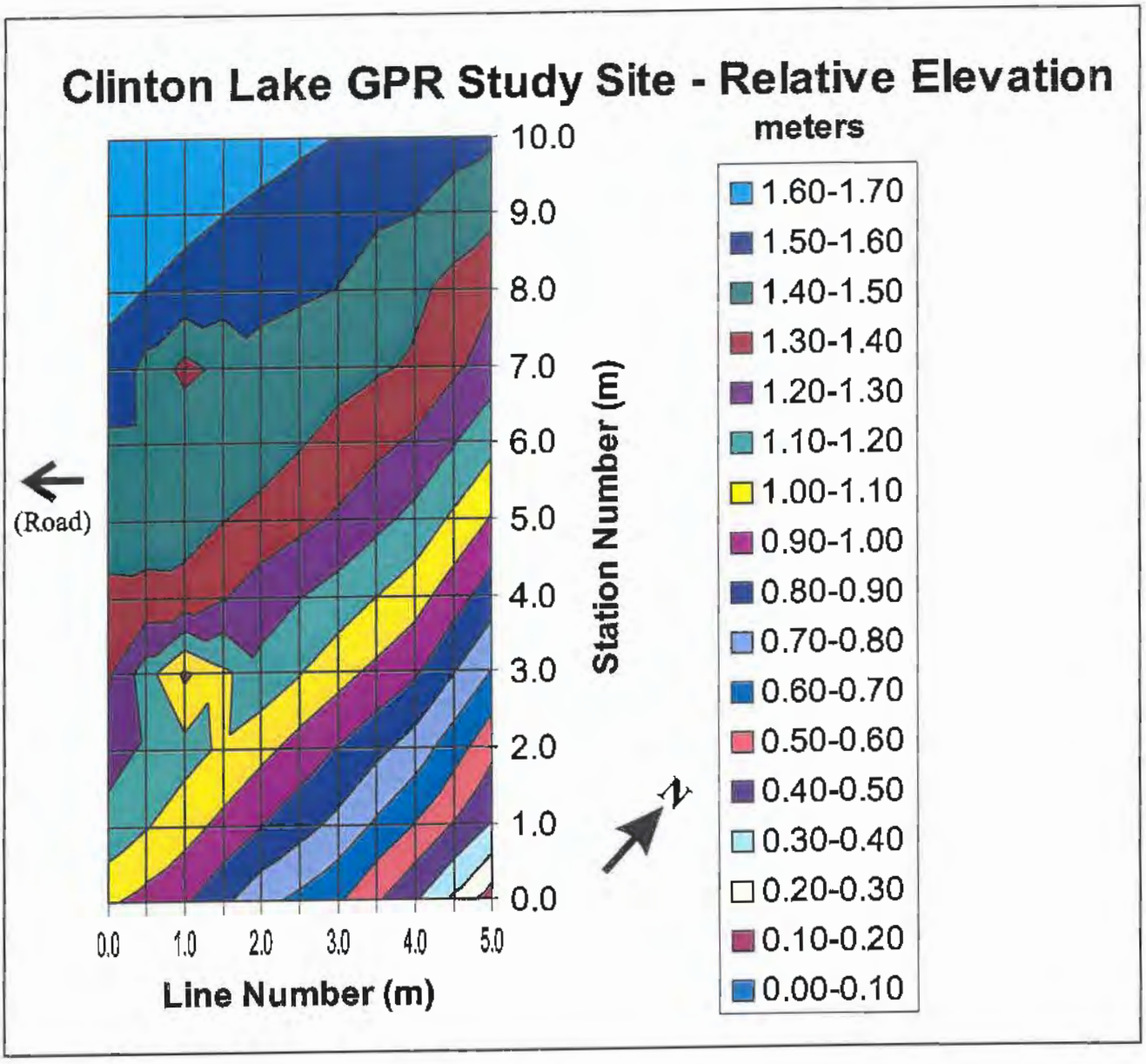

Figure 3. Clinton Lake GPR study site.

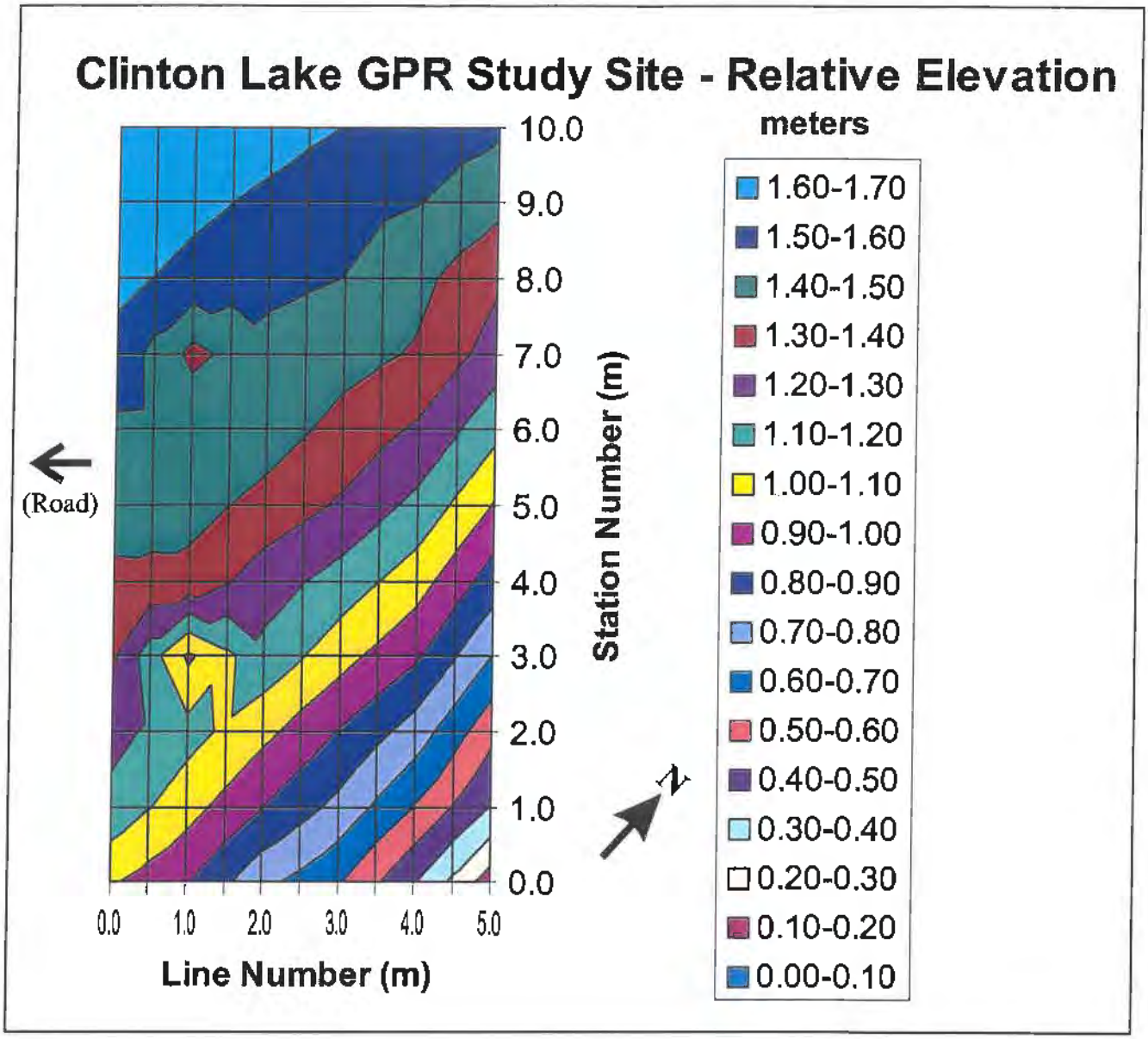

Figure 3. Clinton Lake GPR study site.

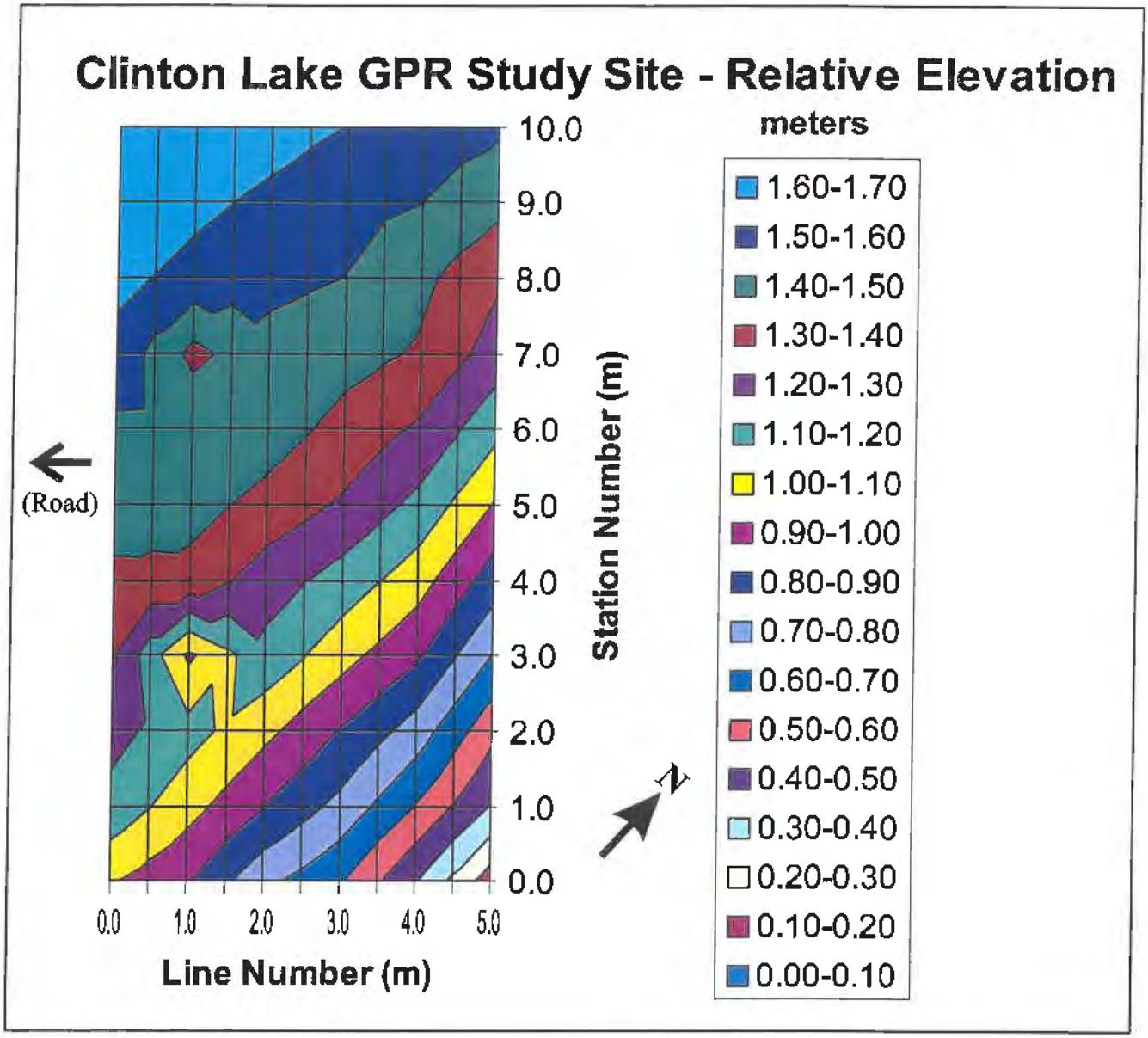

Figure 3. Clinton Lake GPR study site.

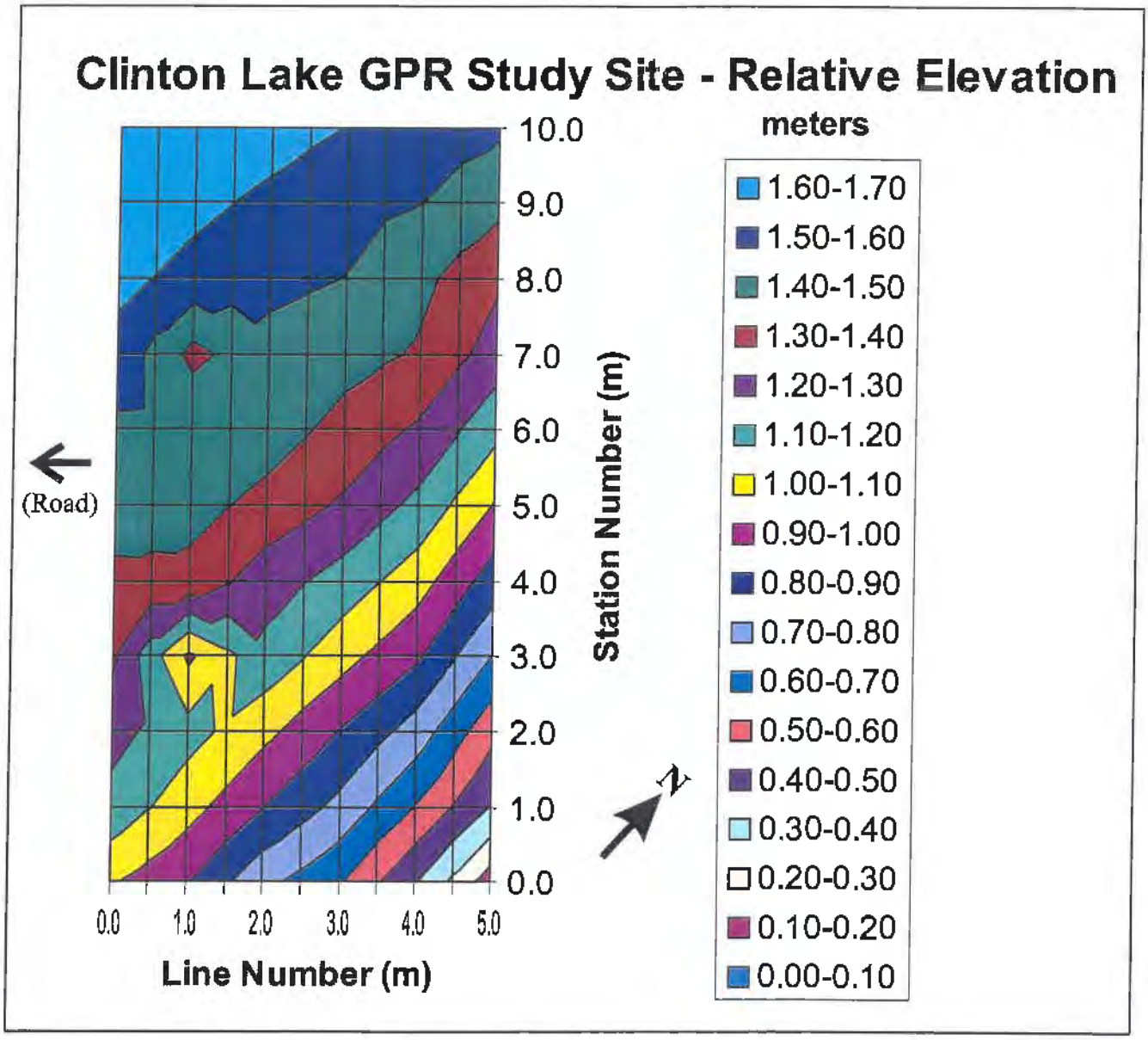

Figure 3. Clinton Lake GPR study site.